Phys Chem Minerals (2006) 33: 73–83
DOI 10.1007/s00269-006-0069-y

ORIGINAL PAPER

Ruslan P. Liferovich · Roger H. Mitchell

Tantalum-bearing titanite: synthesis and crystal structure data

Received: 12 July 2005 / Accepted: 18 September 2005 / Published online: 8 March 2006

Abstract Synthetic titanite, $CaTiOSiO_4$, and the series of $(Ca_{1-x}Na_x)(Ti_{1-x}Ta_x)OSiO_4$ and $Ca(Ti_{1-2x}Ta_xAl_x)OSiO_4$ solid solutions have been prepared by ceramic methods, and their crystal structure determined by the Rietveld analysis. At ambient conditions, titanite can contain up to 20 mol% $NaTaOSiO_4$ or 60 mol% $Ca(Al_{0.5}Ta_{0.5})OSiO_4$. These limits might differ in natural samples due to combination with substitutions involving fluorine and/or hydroxyl replacing oxygen together with vacancies at cationic sites. All cations located at the ^{vii}X- and ^{vi}Y-sites in the structures of tantalian titanite are disordered. Expansion of the <Si–O> bond from 1.618 to 1.621 Å in $CaTi_{0.8}Ta_{0.1}Al_{0.1}OSiO_4$ and $CaTi_{0.6}Ta_{0.2}Al_{0.2}OSiO_4$ to 1.644 Å in the $CaTi_{0.4}Ta_{0.3}Al_{0.3}OSiO_4$ titanite suggests the possible presence of some Al^{3+} in the tetrahedral site replacing Si^{4+} in the latter. All tantalian titanites crystallize in the space group $A2/a$. This implies that both single-site and complex double-site substitutional schemes induce $P2_1/a \rightarrow A2/a$ phase transition(s). The $(Ca_{1-x}Na_x)(Ti_{1-x}Ta_x)OSiO_4$ substitution scheme incorporates larger cations at both the ^{vii}X and ^{vi}Y sites, whereas the $Ca(Ti_{1-2x}Ta_xAl_x)OSiO_4$ scheme involves only ^{vi}Y-site (Al^{3+},Ta^{5+}) cations with a slightly smaller "average" radius. Unit cell dimensions change insignificantly or increase incrementally with increase of average cationic radii in the $(Ca_{1-x}Na_x)(Ti_{1-x}Ta_x)OSiO_4$ series, and with an insignificant decrease in the $^{vi}R_Y$ average cationic radii in the $Ca(Ti_{1-2x}Ta_xAl_x)OSiO_4$ series. Both Ta-doped titanite and $CaTiOSiO_4$ consist of distorted polyhedra with the XO_7, YO_6 coordination polyhedra and the SiO_4 tetrahedron in tantalian titanite being less distorted compared to those of the pure $CaTiOSiO_4$.

R. P. Liferovich · R. H. Mitchell (✉)
Department of Geology, Lakehead University,
955 Oliver Road, P7B 5E1, Thunder Bay, Ontario, Canada
E-mail: rmitchel@lakeheadu.ca
Tel.: +1-807-3438287
Fax: +1-807-3467853

Keywords Titanite · Tantalum · Aluminium · Natrium · Crystal structure

Introduction

Titanite, $CaTiOSiO_4$, is an important accessory phase in igneous and metamorphic rocks and a major rock-forming mineral in highly differentiated agpaitic nepheline syenite. Typically, the composition of igneous titanite approaches the theoretical stoichiometry, whereas in contrast, titanite formed during diverse postmagmatic processes is known to incorporate significant amounts of Zr, Nb and Ta (Sahama 1946; Černý and Riva di Sanseverino 1972; Clark 1974; Paul et al. 1981; Woolley et al. 1992; Russel et al. 1994; Černý et al. 1995; Chakhmouradian et al. 2003, 2004; Brigatti et al. 2004; Liferovich and Mitchell 2005a). Niobian titanite occurs primarily in postmagmatic parageneses in nepheline syenite and carbonatite (Chakhmouradian et al. 2003; Chakhmouradian 2004; Brigatti et al. 2004; Liferovich and Mitchell 2005a). Tantalian titanite, commonly also enriched in Nb, is known from siliceous pegmatites, where it typically forms as a product of subsolidus alteration of primary tantalo-niobates (columbite-tantalite, fersmite, ixiolite, microlite, strüverite, etc.) and (Nb,Ta)-rich rutile (Černý and Riva di Sanseverino 1972; Clark 1974; Paul et al. 1981; Černý et al. 1995). Both niobium and tantalum enter the structure of titanite according to two major substitutional schemes (Table 1). In natural titanite these schemes can occur in conjunction with the presence of minor vacancies and/or fluorine or hydroxyl replacing up to one atom of oxygen per a formula unit (*apfu*). The greatest concentration of tantalum in a natural titanite described to date is 21.5 wt% Ta_2O_5 (0.22 *apfu* Ta) in combination with up to 9.49 wt% Nb_2O_5 (0.16 *apfu* Nb), with a maximum of 0.36 *apfu* $(Ta,Nb)_2O_5$ (Černý et al. 1995).

Natural samples of tantalian and niobian titanite are commonly inhomogeneous (Clark 1974; Černý et al. 1995; Chakhmouradian 2004; Liferovich and Mitchell

Table 1 Principal substitutional schemes involving tantalum and niobium in natural titanite

	Niobian titanite	Tantalian titanite
Genesis	Postmagmatic, hydrothermal	
Host rock	Si-undersaturated (nepheline syenites, carbonatites)	Siliceous (granite pegmatites)
	Principal substitutional schemes	
Double site	$^{vii}Ca^{2+} + {}^{vi}Ti^{4+} \rightleftarrows {}^{vii}Na^{+} + {}^{vi}M^{5+}$	
	0.25 *apfu* Nb	0.09 *apfu* Na ($+M^{3+}$, F^{-}, OH^{-})
	0.21 *apfu* Na ($+ \square$, F^{-}, OH^{-})	0.20 *apfu* Ta
Single site	$2{}^{vi}Ti^{4+} \rightleftarrows {}^{vi}M^{3+} + {}^{vi}M^{5+}$	
	0.17 *apfu*Nb ($+ \square$, F^{-}, OH^{-})	0.21 *apfu* Ta (0.36 *apfu* Ta + Nb)
	0.23 *apfu* M^{3+}	0.29 *apfu* Al (0.10 *apfu* Na)

Data used for this compilation are from Sahama (1946), Černý and Riva di Sanseverino (1972), Clark (1974), Paul et al. (1981), Woolley et al. (1992), Russel et al. (1994), Černý et al. (1995), Della Ventura et al. (1999); Chakhmouradian et al. (2003), Chakhmouradian (2004), Brigatti et al. (2004), Liferovich and Mitchell (2005a)
apfu atoms per formula unit, □ vacancy

2005a), and this together with their small crystal size hinders study of their structure using single-crystal methods. Data on the structure of naturally occurring titanite enriched in tantalum and/or niobium is limited to a single-crystal study of titanite from Mt. Somma, Italy containing 0.16 *apfu* $(Al,Fe)^{3+}$ and only 0.04 *apfu* Nb^{5+}, with comparable amounts of Zr^{4+}, OH^{-} and F^{-} (Brigatti et al. 2004). This study showed that single-site $2{}^{vi}Ti^{4+} \rightleftarrows {}^{vi}(Al,Fe)^{3+} + {}^{vi}M^{5+}$ diadochy is primarily responsible for the incorporation of Nb^{5+} into the structure. Crystal structure data on synthetic analogs of titanite enriched in M^{5+} are limited to a niobian titanite with 0.15 *apfu* Nb^{5+}, incorporated by a two-site cationic substitutional scheme, $^{vii}Na^{+} + {}^{vi}M^{5+} \rightleftarrows {}^{vii}Ca^{2+} + {}^{vi}Ti^{4+}$ (Liferovich and Mitchell 2005a). These experimental data indicate that a two-site substitution can result in substitution of considerably more M^{5+} as compared to that occurring in titanite from Mt. Somma, Italy and are in accord with the substitutions found in other examples of natural titanite. Crystal structure data are not available for either natural or synthetic tantalian varieties of titanite.

This contribution reports the first experimental synthesis and crystal structure study of tantalian titanite and a comparison of the response of the titanite structure to single- and two-site substitutions involving Ta.

The structure of titanite

Titanite, $^{vii}X{}^{vi}YO{}^{iv}TO_4$, consists of kinked chains of corner-linked YO_4O_2 octahedra sharing O(1) atoms (Fig. 1). Silicon tetrahedra cross-link the chains of octahedra. This fully corner-linked structure can be considered as a YO_6–SiO_4 polyhedral framework with large cavities enclosing the large X atoms, typically Ca^{2+}, in irregular seven-fold cages.

Description of titanite and its displacive phase transformations have been addressed in detail in numerous publications (Taylor and Brown 1976; Ghose et al. 1991; Van Heurk et al. 1991; Salje et al. 1993; Kunz et al. 1996, 2000; Kek et al. 1997; Angel et al. 1999; Malcherek 2001; Liferovich and Mitchell 2005a, b, c).

In pure titanite at ambient conditions all atoms of titanium occur in off-centre positions displaced in the same direction within an individual chain of octahedra, but in opposite directions between neighbouring chains (Fig. 1a), resulting in antiferroelectric interactions. The displacement of titanium atoms in the structure of low-temperature titanite might result from (1) an electronic second-order Jahn–Teller effect occurring around the octahedrally coordinated cations of this d^0-transition metal (Kunz and Brown 1994); (2) ordering of Ca in the seven-fold site (Kek et al. 1997); (3) underbonding of bridging O(1) anions at anti-phase boundaries (Hughes et al. 1997).

The displacive $P2_1/a \rightarrow A2/a$ phase transition of titanite is stepwise and can be induced by an increase in pressure or temperature. The sequence of the phase transitions is illustrated in Fig. 1a–c (for details refer to Troitzsch and Ellis 2002). The same phase transition occurs as a structural response to elemental substitutions at the single octahedral site as a result of a decrease in the second Jahn–Teller effect and underbonding of the O(1) anions, or can be induced by more complex substitutions involving the seven-fold site (Hughes et al. 1997; Liferovich and Mitchell 2005a, b, c) and bridging oxygen sites (Troitzsch et al. 1999; Brigatti et al. 2004). Conventionally, the $\alpha \rightarrow \beta$ transformation (Fig. 1a, b) is termed "the $P2_1/a$ to $A2/a$ phase transition", bearing in mind that it probably does not strictly represent the entire antiferroelectric-to-paraelectric transformation ($\alpha \rightarrow \gamma$; Fig. 1a, c) and is due to long-range disorder of the "titanium–oxygen" dipoles (Fig. 1b) rather than actual centring of the ^{vi}Y cations (Troitzsch and Ellis 2002). Recently, Elleman-Olesen and Malcherek (2005) have demonstrated that further distortion of the XYO-TO_4 structure results in a transition from the monoclinic space group $A2/a$ to the triclinic space group $A\bar{1}$, which might be considered as a "$\gamma \rightarrow \delta$" transition.

In the fully corner-linked structure of titanite, different polyhedra have differing responses to structural tensions driven by high pressure and temperature. In

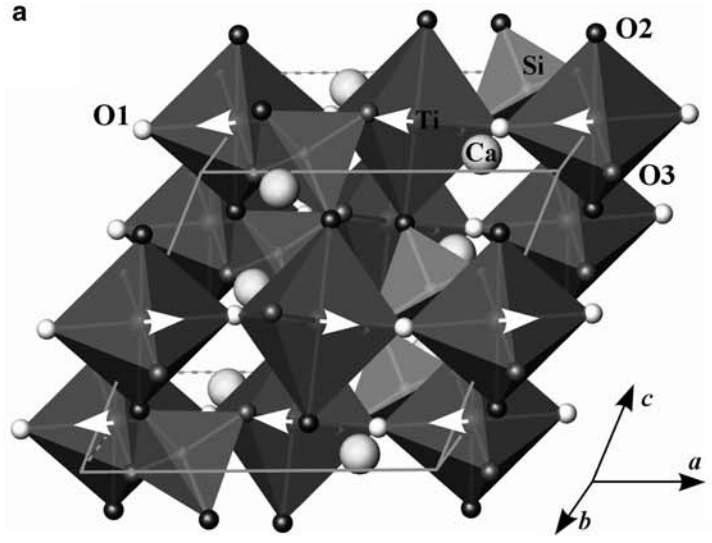

"α"-titanite

T < 496 K for $CaTiOSiO_4$

sp. gr. $P2_1/a$

^{vii}X ordered;

^{vi}Y shifted coherently within a single chain

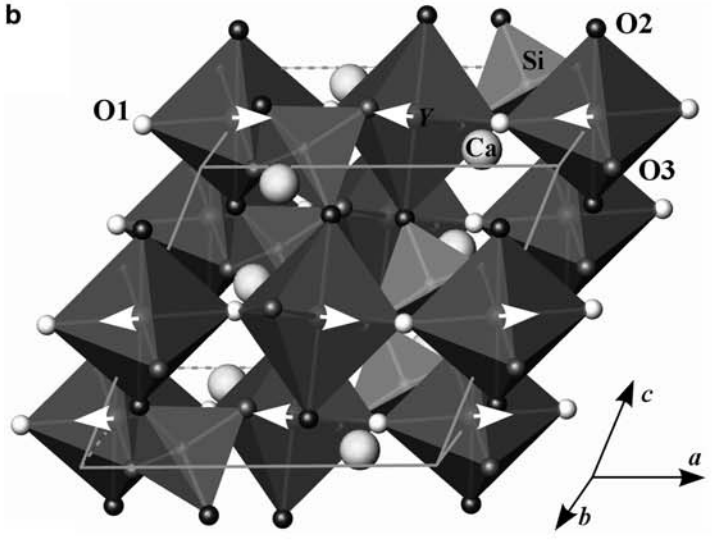

"β"-titanite

? ≤ P ≤ 3.5 GPa

or 496 < T < 825 K

sp. gr. quasi - *A2/a* (with $P2_1/a$ domains at unit-cell scale)

^{vii}X in split position;

long-range disorder between ^{vi}Y-O(1) dipoles

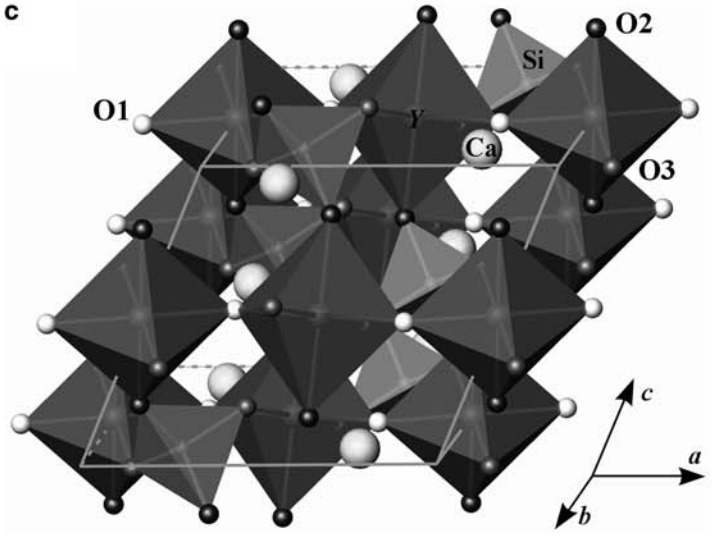

"γ"-titanite

P ≥ 3.5 GPa

or T > 825 K

sp. gr. A2/a

^{vii}X oscillates;

^{vi}Y centered

Fig. 1 Crystal structure and phase transitions of titanite. The unit-cell boundaries are outlined. Dipoles within TiO_6 octahedra (**a**, **b**) represent off-centre displacement of six-coordinated atoms from the ideal position observed in the $CaTiOSiO_4$ and not present in Na–Ta- and Al–Ta-doped synthetic titanite (see text for details)

pure $CaTiOSiO_4$, the SiO_4 tetrahedra show a strong angular distortion with only minor change in bond lengths, whereas the polymerized CaO_7 polyhedra are significantly distorted and TiO_6 octahedra rotate rigidly (Kunz et al. 2000). Interactions between the kinked character of the octahedral chains, changes of electronic effects around the six-fold coordinated cations and different style of deformation of different coordination polyhedra in the corner-linked framework are complex. In some instances, this results in seemingly paradoxical responses of the titanite structure to the stresses inducing the deformations. Thus, some bond lengths increase and the octahedral chains straighten and extend with decreasing unit-cell volume at increasing pressures (Kunz et al. 2000).

Here we report the response of the structure of hydroxyl- and fluorine-free tantalian titanite to Ta substitution in the $(Ca_{1-x}Na_x)(Ti_{1-x}Ta_x)OSiO_4$ and $Ca(Ti_{1-2x}Ta_xAl_x)OSiO_4$ solid solution series; the commonest occurring in natural samples (Table 1). These solid solution series have been investigated at increments of 0.1 *apfu* Ta to determine the limits of Ta substitution at ambient conditions.

Synthesis and analytical technique

The samples were prepared by a solid-state ceramic method from stoichiometric amounts of $CaSiO_3$ (wollastonite polymorph 1*A*), TiO_2, Ta_2O_5, Al_2O_3 and Na_2CO_3 (the latter was taken in 5 mol% excess to compensate for volatilization of Na), purchased from the Alfa Aesar Chemical Co. The pure titanite end member, $CaTiOSiO_4$, was also prepared as a reference material. The reagents, dried at 120°C for several days, were mixed, ground in an agate mortar under acetone, and calcined in air for 24 h at 1,000°C. After regrinding for 1 h, the samples were pelletized at a pressure of 10 ton/cm^2. Al–Ta titanites were prepared by a two-step sintering in air for 96 h at 1,175°C with further grinding (and pelleting) after the first 48 h and quenching in air. Preparation of the Na–Ta titanites was more challenging, as the samples remained inhomogeneous when prepared according to the above sintering procedure. An increase in the time of synthesis resulted in volatilization of significant amounts of Na. Attempts at synthesis using more Na in the initial mixtures and/or by the introduction of Na to the intermediate products resulted in the formation of complex sodic perovskites and sodic silicate phases. Experiments with complete melting and quenching of the samples followed by sintering of the glassy product (Speer and Gibbs 1976; Hughes et al. 1997; Chakhmouradian 2004) were not successful for the Na–Ta compounds. Eventually, these were prepared by heating dense-pelletized initial mixtures (20 ton/cm^2) to 1,225°C, that is well above of their melting points, for a short time (no longer than 5 min), resulting in partial melting only of the outermost parts of the samples. The Na–Ta compounds were then cooled to 1,175°C, at a rate of 10°C/min and sintered for 96 h followed by quenching to room temperature. Subsequently, the glassy covering material was mechanically removed and the remaining homogeneous material used for this study.

In this work, we employ the analytical procedures of quantitative energy-dispersive X-ray spectrometry (QEDS SEM), powder X-ray diffractometry (XRD) and Rietveld refinement methods which have been described in detail by Liferovich and Mitchell (2005a, b, c).

Tantalian titanite

The tantalian titanite synthesized here consisted of fine-grained (average, 20 μm) aggregates containing, in some instances only minor amounts of rutile, rynersonite ($CaTa_2O_6$), quartz and/or a compositionally complex orthorhombic perovskite [*Pbnm* (Ca,Na)(Ti,Ta)O_3]. Rietveld refinement data show that the total amount of impurities never exceeds 1.5–3.4 wt%. Synthesis of the entire $(Ca_{1-x}Na_x)(Ti_{1-x}Ta_x)OSiO_4$ and $Ca(Ti_{1-2x}Ta_xAl_x)OSiO_4$ series was attempted, but was successful only for very limited compositional ranges in both series. The titanites $Ca_{0.9}Na_{0.1}Ti_{0.9}Ta_{0.1}OSiO_4$ (hereafter $NaTa_1$), $Ca_{0.8}Na_{0.2}Ti_{0.8}Ta_{0.2}OSiO_4$ ($NaTa_2$), $CaTi_{0.8}Ta_{0.1}Al_{0.1}OSiO_4$ ($AlTa_1$), $CaTi_{0.6}Ta_{0.2}Al_{0.2}OSiO_4$ ($AlTa_2$) and $CaTi_{0.4}Ta_{0.3}Al_{0.3}OSiO_4$ ($AlTa_3$) were obtained as compositionally homogeneous compounds as confirmed by quantitative energy-dispersive analyses and back-scattered electron imagery. Compositional data for these compounds agree well with results for refinements of the occupancies of the ^{vii}X and ^{vi}Y sites for the same samples using the Rietveld technique.

For experiments with $x_{NaTa} > 0.2$ and $x_{TaAl} > 0.3$, back-scattered electron images and XRD patterns demonstrated the presence of wollastonite (transformed to the 4*A* polymorph), rutile and complex titanates and niobates. In addition, the abundance of starting material remaining as non-reacted phases increases with x. The titanium-free end member compositions did not form any titanite-structured compounds.

For the synthesized tantalian titanites, high-resolution laboratory X-ray diffractometry does not show the presence of $2\bar{2}\bar{1}$ and $2\bar{1}\bar{2}$ reflections, which are well developed in the high-resolution XRD pattern of pure $CaTiOSiO_4$ (see Liferovich and Mitchell 2005a, b, c for details). Given that extinction rules do not allow "$k + l$ = odd" reflections in the space group $A2/a$, we conclude that entry of tantalum to the titanite structure at ambient pressure by either single- or two-site substitutional schemes results in the stabilization of compounds adopting $A2/a$ symmetry.

Rietveld refinement

Voigt, Pseudo-Voigt and fundamental parameter approaches were tried for fitting the XRD profiles. Finally, the fundamental parameter mode was used for all

refinements as it utilizes a convolution-based profile which reduces the number of definable parameters and thus eliminates many problems related to over-parameterization, particularly the refinement of redundant parameters and parameter correlations [p. 68 in Bruker (2003)]. Another advantage of the fundamental parameter approach to line profile fitting is that the fitted lattice parameters are automatically corrected for the line profile shifts arising from instrumental aberrations (Cheary and Cline 1995). The size of crystallites was estimated using the "Sherrer equation" (Young 1995; Bruker 2003).

Depending upon the presence of impurities, the number of TOPAS 2.1 refined variables ranged up to 44 independent parameters. These included zero corrections, scaling factors, cell dimensions, atomic positional coordinates, preferred orientation corrections, crystal size and strain effects, and isotropic thermal parameters. The background was modelled using a sixth-order Chebyshev polynomial. A fourth-order spherical harmonic series was employed for the correction of preferred orientation effects. The starting site populations were set with the target composition of the synthesis, and refined at the final steps of the procedure. The total occupation of the X and Y sites was constrained to unity.

For Rietveld refinement of $CaTiOSiO_4$, we used the atomic coordinates given by Kek et al. (1997) as a starting model, and those given by Kunz et al. (1997) for $A2/a$-structured Ta-bearing titanite. Figure 2 is a portion of the Rietveld refinement plot for the synthetic $CaTi_{0.8}Ta_{0.1}Al_{0.1}OSiO_4$ titanite ($AlTa_1$) over the 2θ range from 15° to 80° (note that the actual refinement is over the $2\theta = 9°–145°$ range).

Given the small volume fractions of the minor contaminant phases (Table 2), the atomic coordinates for these phases were fixed during the refinements. Restraints for bond lengths of the coordination octahedra or tetrahedra in the titanites were not applied as refinements converged rapidly. Positional parameters were refined stepwise, from heavier to lighter cations with those of the oxygen anions last. Atomic displacement factors were refined as an isotropic approximation; the factors for different cations occupying the Y-site or X-site were constrained to be equal during refinements. With the above constraints incorporated into the Rietveld routine, refinement is rapid and the correlation between the site occupancies, the scale parameters and the fractional coordinates is small. As a final step in the refinement procedure, we attempted to refine occupancies of the seven-fold, octahedral and tetrahedral sites. The refinements converged easily (in a few steps) and did not induce any statistically significant changes in any of the refined parameters. Obtained site occupancies do not deviate from the target stoichiometries within the range of one e.s.d. (estimated standard deviation) within the accuracy of Rietveld method. Results of the site occupancy refinement show that all cations located at the ^{vii}X- and ^{vi}Y-sites are disordered and do not indicate the presence of tetrahedrally coordinated Al^{3+} in aluminoan–tantalian titanite, or vacancies at cationic sites within the accuracy of the Rietveld method.

Agreement factors and unit-cell parameters are given in Table 2. Crystal structure parameters for Ta-bearing sodic and aluminoan titanite are listed in Table 3 in comparison with the parameters obtained for the pure $CaTiOSiO_4$. The latter are close to those determined for

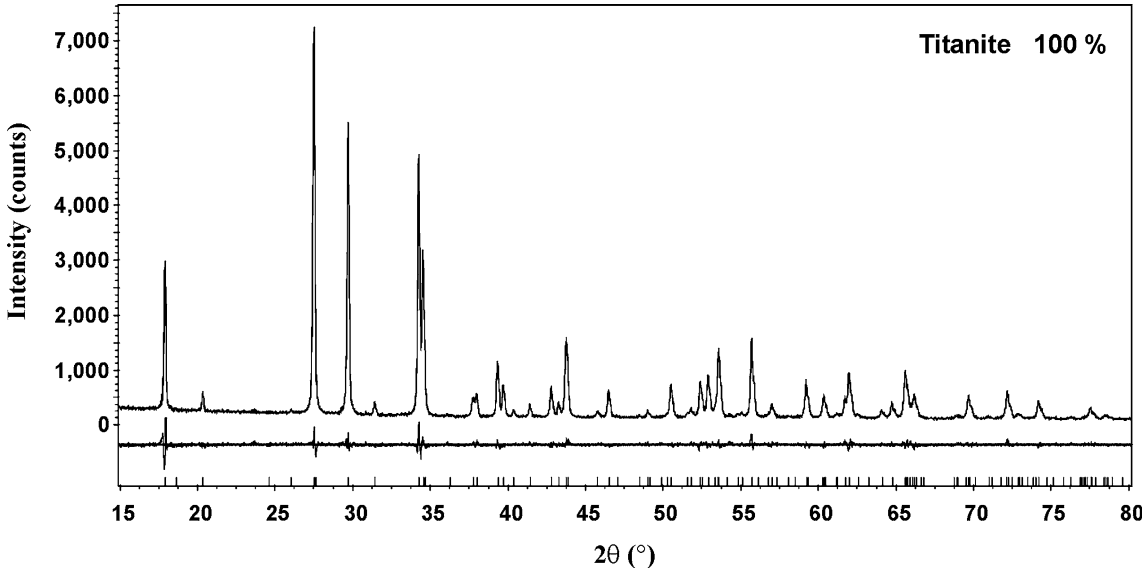

Fig. 2 A portion of the Rietveld refinement plot (*line*) of the X-ray powder diffraction data for $CaTi_{0.8}Ta_{0.1}Al_{0.1}OSiO_4$ synthetic titanite at room temperature (*dots*). For agreement factors see Table 2. *Note*: the whole-range diffraction pattern ($2\theta = 9°–145°$) was employed for the refinement purpose

Table 2 Rietveld refinement data for synthetic titanite ($P2_1/a$) and tantalian titanite ($A2/a$)

	$CaTiOSiO_4$	$NaTa_1$	$NaTa_2$	$AlTa_1$	$AlTa_2$	$AlTa_3$
Titanite (%)	98.1(3)	99.6(1)	97.3(2)	100	99.3(1)	97.8(1)
Others (%)	*Ru* 1.9(3)	*Per* 0.4(1)	*Ru* 1.5(2) *Per* 1.2(1)	–	SiO_2 0.7(1)	*Ryners* 2.2(1)
a (Å)	7.0599(1)[a]	7.0826(1)	7.1122(1)	7.0547(1)	7.0610(1)	7.0699(1)
b (Å)	8.7156(1)[a]	8.7156(1)	8.7166(1)	8.7121(1)	8.7162(2)	8.7220(2)
c (Å)	6.5597(1)[a]	6.5767(1)	6.5962(1)	6.5629(1)	6.5697(1)	6.5776(1)
β (°)	113.797(1)[a]	113.911(1)	114.078(1)	113.750(1)	113.742(1)	113.744(2)
V ($Å^3$)	369.30(1)[a]	371.14(1)	373.34(1)	369.20(1)	370.11(1)	371.27(1)
N	36[a]	38	44	34	38	42
R_{wp} (%)	11.50[a]	9.06	7.96	8.62	7.53	6.83
R_{Bragg} (%)	3.0[a]	3.30	2.44	2.52	2.41	2.16
R_{exp} (%)	8.78[a]	6.67	5.65	6.51	5.59	5.10
R_p (%)	6.88[a]	7.12	6.20	6.68	5.91	5.33
GoF	1.31[a]	1.36	1.41	1.32	1.35	1.34
DW	1.26[a]	1.17	1.16	1.25	1.18	1.19

$CaTiOSiO_4$ this study; $NaTa_1$ $Ca_{0.9}Na_{0.1}Ti_{0.9}Ta_{0.1}OSiO_4$; $NaTa_2$ $Ca_{0.8}Na_{0.2}Ti_{0.8}Ta_{0.2}OSiO_4$; $AlTa_1$ $CaTi_{0.8}Ta_{0.1}Al_{0.1}OSiO_4$; $AlTa_2$ $CaTi_{0.6}Ta_{0.2}Al_{0.2}OSiO_4$; $AlTa_3$ $CaTi_{0.4}Ta_{0.3}Al_{0.3}OSiO_4$
Ru rutile; *Per* orthorhombic (*sp. gr. Pbnm*) perovskite; *SiO*$_2$ quartz; *Ryners* rynersonite ($CaTa_2O_6$)
n number of refined parameters

$$R_{wp} = \{[\Sigma_{w_i}(y_{i(obs)} - y_{i(calc)})^2]/[\Sigma_{w_i}(y_{i(obs)})^2]\}^{1/2}$$

$$R_{Bragg} = (\sum |I^{1/2}_{k(obs)} - I^{1/2}_{k(calc)}|)/(\sum I^{1/2}_{k(obs)})$$

$$R_p = [\sum w_i|y_{i(obs)} - y_{i(calc)}|]/\sum y_{i(obs)}$$

$$R_{exp} = [(N-P)/(\sum w_i y^2_{i(obs)})]^{1/2}$$

$$DW \text{ (Durbin–Watson statistic)} = [\textstyle\sum_{i=2}^{N}(\Delta y_i - \Delta y_{i-1})^2]/\sum_{i=1}^{N}\Delta y_i^2$$

$$GoF = \chi^2 = [\textstyle\sum w_i(y_{i(obs)} - y_{i(calc)})^2]/(N-P)$$

[a]Parameters for the $P2_1/a$-structured compound

Table 3 Crystal structure parameters for synthetic titanite ($P2_1/a$) and tantalian titanite ($A2/a$)

	$CaTiOSiO_4$	$NaTa_1$	$NaTa_2$	$AlTa_1$	$AlTa_2$	$AlTa_3$
$<X–O>$ (Å)	2.463(12)[a]	2.469(14)	2.472(14)	2.462(12)	2.468(15)	2.472(17)
V_{XO7} ($Å^3$)	19.887[a]	20.195	20.490	20.020	20.136	20.048
Δ_7	2.90[a]	1.76	1.86	1.81	1.72	1.26
$<Y–O>$ (Å)	1.966(14)[a]	1.972(8)	1.973(8)	1.962(8)	1.959(8)	1.948(10)
V_{YO6} ($Å^3$)	10.095[a]	10.190	10.208	10.042	9.994	9.830
d_Y	0.060[a]	–	–	–	–	–
∂_{xY}	0.009[a]	–	–	–	–	–
∂_{yY}	0.000[a]	–	–	–	–	–
∂_{zY}	0.003[a]	–	–	–	–	–
Δ_6	2.35[a]	1.41	1.43	1.38	1.37	1.24
δ_6	2.56[a]	1.99	0.93	2.32	0.76	1.07
$<Si–O>$ (Å)	1.622(14)[a]	1.613(11)	1.609(11)	1.618(10)	1.621(12)	1.644(14)
V_{SiO4} ($Å^3$)	2.177[a]	2.135(4)	2.125	2.159	2.169	2.263
Δ_4	0.19[a]	0.05	0.04	0.03	0.09	0.18
δ_4	17.24[a]	19.73	13.74	19.48	17.79	16.79
Ti–O1–Ti (°)	143.2[a]	143.0	144.1	143.1	144.0	145.4
Si–O2–Ti (°)	139.5[a]	141.4	143.1	141.3	141.9	141.8
Si–O3–Ti (°)	142.5[a]	128.8	128.4	128.8	129.4	128.8
Si–O4–Ti (°)	130.1[a]	–	–	–	–	–
Si–O5–Ti (°)	128.1[a]	–	–	–	–	–

$CaTiOSiO_4$ this study; $NaTa_1$ $Ca_{0.9}Na_{0.1}Ti_{0.9}Ta_{0.1}OSiO_4$; $NaTa_2$ $Ca_{0.8}Na_{0.2}Ti_{0.8}Ta_{0.2}OSiO_4$; $AlTa_1$ $CaTi_{0.8}Ta_{0.1}Al_{0.1}OSiO_4$; $AlTa_2$ $CaTi_{0.6}Ta_{0.2}Al_{0.2}OSiO_4$; $AlTa_3$ $CaTi_{0.4}Ta_{0.3}Al_{0.3}OSiO_4$
d_Y the displacement of the central atom; ∂_{xY}, ∂_{yY} and ∂_{zY} components of the vector of ^{vi}Y atom displacement
[a]Parameters for the $P2_1/a$-structured compound

synthetic titanite obtained by synchrotron radiation data (Kek et al. 1997). Atomic positional parameters and atomic displacement factors obtained for tantalian titanites, are listed in Table 4, with selected bond lengths given in Table 5.

Table 4 Positional and atomic displacement factors for synthetic titanite ($P2_1/a$) and tantalian titanite ($A2/a$)

Position	Sample	*x*	y	z	B_{iso} (Å^2)
^{vii}X	$CaTiOSiO_4$	0.2573(8)[a]	0.4184(3)[a]	0.2477(10)[a]	1.43(7)[a]
	$NaTa_1$	1/4	0.1693(3)	0	1.44(9)
	$NaTa_2$	1/4	0.1693(4)	0	1.22(1)
	$AlTa_1$	1/4	0.1690(3)	0	1.50(9)
	$AlTa_2$	1/4	0.1694(4)	0	1.86(1)
	$AlTa_3$	1/4	0.1695(4)	0	1.97(13)
^{vi}Y	$CaTiOSiO_4$	0.4846(5)[a]	0.2478(8)[a]	0.7519(7)[a]	0.88(7)[a]
	$NaTa_1$	1/2	0	1/2	0.70(5)
	$NaTa_2$	1/2	0	1/2	0.56(8)
	$AlTa_1$	1/2	0	1/2	0.65(4)
	$AlTa_2$	1/2	0	1/2	0.54(4)
	$AlTa_3$	1/2	0	1/2	0.45(4)
^{iv}Si	$CaTiOSiO_4$	0.7434(10)[a]	0.4319(4)[a]	0.2492(15)[a]	0.60(7)[a]
	$NaTa_1$	3/4	0.1811(4)	0	0.54(14)
	$NaTa_2$	3/4	0.1809(6)	0	0.71(12)
	$AlTa_1$	3/4	0.1807(4)	0	0.75(9)
	$AlTa_2$	3/4	0.1805(6)	0	0.94(12)
	$AlTa_3$	3/4	0.1805(7)	0	1.00(15)
O1	$CaTiOSiO_4$	0.7480(22)[a]	0.3204(6)[a]	0.7552(32)[a]	1.06(6)[a]
	$NaTa_1$	3/4	0.0679(6)	1/2	0.79(7)
	$NaTa_2$	3/4	0.0661(7)	1/2	0.77(8)
	$AlTa_1$	3/4	0.0676(6)	1/2	0.87(7)
	$AlTa_2$	3/4	0.0659(7)	1/2	1.04(8)
	$AlTa_3$	3/4	0.0632(8)	1/2	1.09(9)
O2	$CaTiOSiO_4$	0.9138(15)[a]	0.3202(14)[a]	0.4359(21)[a]	1.06(6)[a]
	$NaTa_1$	0.9088(7)	0.0676(5)	0.1800(7)	0.79(7)
	$NaTa_2$	0.9036(7)	0.0669(5)	0.1822(6)	0.77(8)
	$AlTa_1$	0.9080(6)	0.0658(4)	0.1814(6)	0.87(7)
	$AlTa_2$	0.9076(8)	0.0662(5)	0.1811(6)	1.04(8)
	$AlTa_3$	0.9110(9)	0.0671(6)	0.1838(7)	1.09(9)
O3	$CaTiOSiO_4$	0.0939(16)[a]	0.1869(14)[a]	0.0712(21)[a]	1.06(6)[a]
	$NaTa_1$	0.3853(8)	0.2135(5)	0.4051(7)	0.79(7)
	$NaTa_2$	0.3836(8)	0.2148(5)	0.4039(8)	0.77(8)
	$AlTa_1$	0.3847(7)	0.2126(4)	0.4041(7)	0.87(7)
	$AlTa_2$	0.3850(9)	0.2112(5)	0.4046(8)	1.04(8)
	$AlTa_3$	0.3888(10)	0.2096(6)	0.4041(9)	1.09(9)

$CaTiOSiO_4$ this study; $NaTa_1$ $Ca_{0.9}Na_{0.1}Ti_{0.9}Ta_{0.1}OSiO_4$; $NaTa_2$ $Ca_{0.8}Na_{0.2}Ti_{0.8}Ta_{0.2}OSiO_4$; $AlTa_1$ $CaTi_{0.8}Ta_{0.1}Al_{0.1}OSiO_4$; $AlTa_2$ $CaTi_{0.6}Ta_{0.2}Al_{0.2}OSiO_4$; $AlTa_3$ $CaTi_{0.4}Ta_{0.3}Al_{0.3}OSiO_4$
[a]Parameters for the $P2_1/a$-structured compound

Table 5 Selected bond lengths for synthetic titanite ($P2_1/a$) and tantalian titanite ($A2/a$)

	$CaTiOSiO_4$		$NaTa_1$	$NaTa_2$	$AlTa_1$	$AlTa_2$	$AlTa_3$
X–O1	2.293(5)[a]	*X*–O1	2.290(6)	2.306(7)	2.295(6)	2.308(7)	2.332(8)
X–O2	2.430(12)[a]	2x *X*–O2	2.419(5)	2.409(5)	2.403(4)	2.409(5)	2.430(6)
X–O3	2.402(12)[a]	2x *X*–O3	2.469(5)	2.468(5)	2.460(4)	2.463(5)	2.460(5)
X–O4	2.394(14)[a]	2x *X*–O3′	2.607(5)	2.620(6)	2.607(5)	2.611(6)	2.595(7)
X–O4′	2.752(12)[a]						
X–O5	2.471(15)[a]						
X–O5′	2.499(12)[a]						
Y–O1	1.755(14)[a]	2x *Y*–O1	1.867(2)	1.869(2)	1.859(2)	1.856(2)	1.851(2)
Y–O1′	1.978(14)[a]	2x *Y*–O2	2.023(4)	2.008(4)	2.007(4)	2.008(4)	1.990(5)
Y–O2	2.011(15)[a]	2x *Y*–O3	2.025(4)	2.041(4)	2.019(4)	2.012(4)	2.002(5)
Y–O3	2.007(15)[a]						
Y–O4	2.024(13)[a]						
Y–O5	2.018(13)[a]						
Si–O2	1.619(12)[a]	2x Si–O2	1.601(5)	1.598(5)	1.610(4)	1.606(5)	1.621(6)
Si–O3	1.602(12)[a]	2x Si–O3	1.624(6)	1.619(7)	1.627(6)	1.636(7)	1.665(8)
Si–O4	1.608(16)[a]						
Si–O5	1.659(16)[a]						

$CaTiSiO_5$ this study; $NaTa_1$ $Ca_{0.9}Na_{0.1}Ti_{0.9}Ta_{0.1}OSiO_4$; $NaTa_2$ $Ca_{0.8}Na_{0.2}Ti_{0.8}Ta_{0.2}OSiO_4$; $AlTa_1$ $CaTi_{0.8}Ta_{0.1}Al_{0.1}OSiO_4$; $AlTa_2$ $CaTi_{0.6}Ta_{0.2}Al_{0.2}OSiO_4$; $AlTa_3$ $CaTi_{0.4}Ta_{0.3}Al_{0.3}OSiO_4$
[a]Parameters for the $P2_1/a$-structured compound

Geometry of sites in synthetic tantalian titanite

The $(Ca_{1-x}Na_x)(Ti_{1-x}Ta_x)OSiO_4$ substitution scheme incorporates larger cations at both the ^{vii}X and ^{vi}Y sites, whereas the $Ca(Ti_{1-2x}Ta_xAl_x)OSiO_4$ scheme involves only (Ta^{5+},Al^{3+}) cations with a slightly smaller "average" radius (Shannon 1976) at the ^{vi}Y-site. Our data show that substitution of Ta following both the single- and double-site substitutional schemes induces regular incremental changes in the unit cell dimensions (Table 2). These are considerable for a, b, c, and V, and negligible for the angle of monoclinic distortion, β, in the $Ca(Ti_{1-2x}Ta_xAl_x)OSiO_4$ series (Table 3). A decrease in unit cell parameters which might be expected for the single-site diadochy according to the 1.21 Å ($= 2^{vi}R^{4+}_{Ti}$) → 1.18 Å ($= {}^{vi}R^{5+}_{Ta} + {}^{vi}R^{3+}_{Al}$) scheme is observed for the a and b unit-cell dimensions and V, only in the $AlTa_1$ titanite.

The mean <cation–oxygen> distances within the XO_7 and YO_6 coordination polyhedra vary insignificantly (Table 3). The $<X$–O> distances are similar for all the titanites synthesized and to that of pure $CaTiOSiO_4$ as described by Kek et al. (1997). Entry of Ta^{5+} to the ^{vi}Y site, which is slightly larger than Ti^{4+} ($^{vi}R = 0.64$ and 0.605 Å, respectively; Shannon 1976), affects the $<Y$–O> distances in the NaTa-doped titanite insignificantly, inducing expansion of this distance from 1.966(4) Å ($CaTiOSiO_4$, Table 3) to 1.972–1.973(8) Å, i.e. comparable to precision of the determination. The replacement of Ti^{4+} by the slightly smaller "average atom" ($Al_{0.5}$,$Ta_{0.5}$) induces a regular decrease in the $<Y$–O> distance with increasing x_{AlTa} (Table 3). The volume of the YO_6 coordination polyhedra in the $(Ca_{1-x}Na_x)(Ti_{1-x}Ta_x)OSiO_4$ series is greater than that in pure $CaTiOSiO_4$, and varies insignificantly with x_{NaTa}. The volume of the YO_6 coordination polyhedra in the $Ca(Ti_{1-2x}Ta_xAl_x)OSiO_4$ series decreases with x_{TaAl} (Table 3).

The volume of the XO_7 coordination polyhedron in the $Ca(Ti_{1-2x}Ta_xAl_x)OSiO_4$ series (Table 3) increases regularly for $AlTa_1$ and $AlTa_2$ titanites relatively to that of $CaTiOSiO_4$. This trend is not followed by the $AlTa_3$ sample, as this titanite has a smaller XO_7 volume than that of the $AlTa_2$ titanite. The volume of the XO_7 coordination polyhedron in the $(Ca_{1-x}Na_x)(Ti_{1-x}Ta_x)OSiO_4$ series increases regularly with x_{NaTa} as a result of introduction of the larger $^{vii}Na^+$ cation (Table 3).

The volume of the SiO_4 tetrahedron and the mean <Si–O> bond length in the Ta-bearing titanites are slightly less than, or comparable to, that of $CaTiOSiO_4$ (Table 3). The dimensions of the SiO_4 tetrahedron decrease slightly with x_{NaTa} in the case of the double-site substitution (Table 3), and are not affected by the single-site substitution involving equal amounts of Al and Ta at the octahedral site for $AlTa_1$ and $AlTa_2$. The $AlTa_3$ titanite has a longer <Si–O> bond length and larger SiO_4 volume (Table 3).

The distortion index introduced by Shannon (1976) is useful to illustrate polyhedron bond length distortion, i.e. $\Delta_n = (1/n)[\sum(r_i - \bar{r})/\bar{r}]^2 \times 10^3$, where r_i and $\bar{r}$ are individual and average bond lengths in the polyhedron, respectively. The bond length distortion index is a measure of the distortion of polyhedra induced by compression extension of <cation–oxygen> bonds, and/or stretching, which violate the ideal symmetry of an undistorted polyhedron. To characterize deviations from the ideal bond angles in regular polyhedra, we calculate the bond-angle variance index, δ_n, where $\delta_n = [\Sigma(\theta_i - \theta_n)^2]/(n-1)$ and θ_i are the observed bond angles at the central atom of a polyhedron and θ_n is the ideal O–M–O or O–T–O angle in an undistorted polyhedron (Robinson et al. 1971). The bond-angle variance index reflects twisting and/or tilting deformation of coordination polyhedra whose <cation–oxygen> distances may remain equal in length (Robinson et al. 1971) and thus, are similar in terms of bond length variations. Both the Δ_n and δ_n distortion parameters provide specific insights into the complex geometrical distortions of given polyhedra.

The double-site substitutions induce a significant decrease in the bond-length distortion in the tetrahedra as compared to that in the pure titanite. Much lower tetrahedral bond length distortion in the double site-substituted tantalian titanites (Table 3) also well agrees with some shortening of these bonds and demonstrates that the tetrahedra are not stretched in the Na–Ta titanites.

In the case of single-site substitutions, the tetrahedral bond-length distortion is minimal for the sample with the lowest x_{TaAl} and increases regularly with x_{TaAl} and approaches that of $CaTiOSiO_4$ for the most Al–Ta rich titanite, $AlTa_3$ (Table 3). This observation is in good agreement with the increase of the mean <Si–O> bond lengths and suggests that tetrahedra in the $Ca(Ti_{1-2x}Ta_xAl_x)OSiO_4$ series are distorted due to extension of <cation–oxygen> bonds and/or stretching of the tetrahedra as a bridging element of the framework structure.

Observed deviations of the mean tetrahedral bond lengths from that in the Al-free SiO_4 tetrahedron are conventionally used for considering possible Si⇄Al substitutions [i.e. the degree of ordering of Al ($^{iv}R^{3+} = 0.39$ Å) and Si ($^{iv}R^{4+} = 0.26$ Å; values from Shannon 1976) over the tetrahedral sites, T]. A quantitative model has not yet been developed for tetrahedral–octahedral infinite framework structure(s) such as that of titanite, although some semi-quantitative comparisons are possible with well-studied tectosilicates. Thus, the <Si–O> distances in completely ordered anorthite are in the range from 1.608 to 1.617 Å, whereas the <Al-O> distances are in the range 1.742–1.755 Å (Wainwright and Starkey 1971; Ghose et al. 1993). Similar mean <Si–O> distances are described in the following ordered aluminosilicates: lisetite, 1.619, 1.620, 1.622 and 1.623 Å (Rossi et al. 1986); slawsonite (1.624 Å; Griffen et al. 1977); paracelsian (1.613 Å;

Chiari et al. 1985); and nepheline (1.603–1.616 Å; Tait et al. 2003). Hence, the expansion of the <Si–O> distances from 1.618(10), 1.621(12) Å for the $AlTa_1$ and $AlTa_2$ samples, to 1.644(14) Å and for the $AlTa_3$ sample, might suggest incipient Si⇄Alsubstitution at the tetrahedral site in the case of the most tantaloan–aluminoan titanite. This problem cannot be resolved by using laboratory X-ray powder diffraction methods.

Tetrahedral bond angle variations (δ_4) decrease with x in both series and are similar to those of $CaTiOSiO_4$ (Table 3) for the $AlTa_3$ titanite, but higher for $AlTa_1$ and $AlTa_2$ titanites, and much lower for the $NaTa_2$ titanite. This indicates that twisting and/or tilting deformation of the coordination tetrahedra is relatively high for titanites doped with 0.1 *apfu* Ta and decreases with further substitution by Ta.

The Δ_7 and Δ_6 bond length distortion parameters (Table 3) show also that doping titanite with Ta diminishes the linear distortions of both the seven- and six-fold coordination polyhedra as compared to the distorted polyhedra in $CaTiOSiO_4$ due to the stabilization of the $A2/a$ dimorph resulting from the centring or pseudo-centring of the Y cation in the octahedral site. Octahedral bond angle variations (δ_6), which are significant in pure titanite, $CaTiOSiO_4$, also are reduced by both single- and double-site substitutions (Table 3). This feature was not expected to be found for the $A2/a$-structured titanite dimorph(s) as centring/pseudo-centring of the ^{vi}Y cation and change in average size due to cationic substitution(s) must reduce distortion of the octahedral bond lengths, but not necessarily the twisting and/or tilting deformation of the octahedra. Kinking of the chains of octahedra in Ta-bearing synthetic titanite, as indicated by the pivoting Ti–O(1)–Ti angle (Table 3), increases regularly in both $(Ca_{1-x}Na_x)(Ti_{1-x}Ta_x)OSiO_4$ and $Ca(Ti_{1-2x}Ta_xAl_x)OSiO_4$ series as compared to $CaTiOSiO_4$.

Conclusion

The response of the crystal structure of titanite to cationic substitutions involving $^{vi}Ta^{5+}$ has been studied in the $(Ca_{1-x}Na_x)(Ti_{1-x}Ta_x)OSiO_4$ and $Ca(Ti_{1-2x}Ta_xAl_x)OSiO_4$ solid solution series. Our data demonstrate that (OH,F)-free titanites doped with Ta via both a single-site or a complex two-site substitutional scheme at $x_{Na\text{-}Ta} = 0.1–0.2$, and $x_{TaAl} = 0.1–0.3$, adopt the space group $A2/a$. Both the single- and two-site substitutional schemes affect the coherency of the off-centring of the ^{vi}Y atoms in the chains of octahedra and result in an displacive antiferroelectric-to-paraelectric transition. In part, our study confirms the previously published data regarding an easily inducible phase transition for titanite which can be driven by replacement of only 0.05 *apfu* $^{vii}Ca^{2+}$ and 0.05 *apfu* $^{vi}Ti^{4+}$ (Hughes et al. 1997) and/or by substitutions in the range of 0.09–0.18 *apfu* $^{vi}Ti^{4+}$ and $O(1)^{2-}$ by the same amount of $^{vi}(Al,Fe)^{3+}$ and $(OH,F)^{-}$, respectively (Troitzsch et al. 1999). Conclusions regarding the nature of the centring of the ^{vi}Y atom in Ta-rich titanite and thus discrimination between the $A2/a$-structured "β" and "γ" phases introduced by Troitzsch and Ellis (2002) are not possible on the basis of routine X-ray powder diffraction data.

The seven-fold coordination polyhedra and octahedra in the Ta-doped titanites are less distorted even in the $(Ca_{1-x}Na_x)(Ti_{1-x}Ta_x)OSiO_4$ series involving the larger $^{vii}Na^{+}$ and $^{vi}Ta^{5+}$ than those of pure $CaTiOSiO_4$. Distortion of the SiO_4 tetrahedron is more complex. Generally, this is less distorted in Ta-doped titanite than in $CaTiOSiO_4$, although in the most tantalian sample synthesized, $CaTi_{0.4}Ta_{0.3}Al_{0.3}OSiO_4$, the tetrahedral bond-length distortion is high and similar to that of the pure titanite. Given the significant increase in the mean tetrahedral bond length in this titanite, the presence of some ^{iv}Al might be inferred.

The response of the titanite crystal structure to Ta substitution is seemingly paradoxical in the aluminoan–tantalian series. A regular increase in unit cell parameters is to be expected for the $(Ca_{1-x}Na_x)(Ti_{1-x}Ta_x)OSiO_4$ series involving larger cations at both the seven-fold and octahedral framework sites. In contrast, the $Ca(Ti_{1-2x}Ta_xAl_x)OSiO_4$ solid solution is thought to involve only smaller "average size" cations at the single octahedral site, nevertheless in the case of $AlTa_3$ titanite this "average size" might be in some extent affected by partition of Al into tetrahedral site. Instead of the expected regular decrease of unit cell parameters, the $Ca(Ti_{1-2x}Ta_xAl_x)OSiO_4$ series clearly demonstrates incremental changes in these parameters in most of the samples. In contrast, the volume of the YO_6 octahedra and the mean <Y–O> bond lengths decrease with x_{AlTa} in this series (Table 3), as might be expected on the basis of the substitution of a smaller "average cation" into the octahedron. This observation implies that the Al^{3+} and Ta^{5+} cations ($^{vi}R = 0.535$ and 0.64 Å, respectively; Shannon 1976) are randomly distributed through the octahedral sites in the structure, and act as a "size-averaged cation" only when considered at the scale of the YO_6 polyhedra. On the scale of the whole completely corner linked structure, the random distribution of different size cations induces an effect similar to the entry of a larger cation ($^{vi}Ta^{5+}$) only, and the smaller conjugate cation ($^{vi}Al^{3+}$) does not compensate for expansion of the framework. In particular, the Ti⇄(Al, Ta) substitution not only alleviates deformations of the octahedral site itself, but also diminishes stretching of the tetrahedral site as well as reduces tetrahedral bond angle deformation caused by twisting and/or tilting deformation of the bridging SiO_4. The exact character of this phenomenon is not yet understood and requires a detailed study using precise single crystal structural data.

The empirical limit for entry of Ta to the (F,OH)-free titanite structure at ambient pressure is approximately 0.30 *apfu* Ta in Ta–Al titanite (≈28.9 wt% Ta_2O_5, ≈6.7 wt% Al_2O_3) and approximately 0.20 *apfu* Ta in Na–Ta titanite (≈20.2 wt% Ta_2O_5, ≈2.8 wt% Na_2O).

These limits may differ in natural titanite where concomitant substitutions involving OH^- and/or F^- at the O(1) site or vacancies at the cation sites can occur. The latter is illustrated by the most (Ta,Nb)-rich natural titanite known (Maršikov II pegmatite, Moravia, Czech) which contains up to 0.36 *apfu* $^{vi}(Ta,Nb)^{5+}$. These M^{5+} cations are balanced by only [*apfu*] 0.09 $^{vii}Na^+$ + 0.12 $^{vi}(Al + Fe)^{3+}$ + 0.004 F^- (Černy et al. 1995), thus requiring vacancies with a positive charge deficiency of about 0.15 to maintain neutrality in the structure.

The experimental data show that the existence of a titanite analogue with more than 50 mol% of a $NaTaOSiO_4$ end member is unlikely. The solid solution involving the smaller cations, theoretically might be stabilized at high pressure suggesting the existence of a potentially new compound with ≥67 mol% $Ca(Ta_{0.5}Al_{0.5})OSiO_4$ end member.

Acknowledgements This work is supported by the Natural Sciences and Engineering Research Council of Canada and Lakehead University (Canada). We are grateful to Allan MacKenzie for assistance with the analytical work, and Anne Hammond for sample preparation. Anton Chakhmouradian is thanked for a fruitful discussion regarding the interpretation of data obtained in this work. The authors are grateful to an anonymous reviewer whose constructive criticism resulted in improvements to the initial version of this work. The authors also would like to thank Catherine McCammon for excellent editorial care in her handling of this contribution.

References

Angel RJ, Kunz M, Miletich R, Woodland AB, Koch M, Xirochakis D (1999) High-pressure phase transitions in $CaTiOSiO_4$ titanite. Phase Transit 68:533–543

Brigatti MF, Caprilli E, Mottana A, Poppi L (2004) Nb-containing titanite: new data and crystal structure refinement. Neues Jahrb Mineral Monat 3:117–126

Bruker AXS (2003) TOPAS 2.1: general profile and structure analysis software for powder diffraction data. User's manual. Bruker AXS, Karlsruhe, 79 pp

Černý P, Riva di Sanseverino L (1972) Comments on crystal chemistry of titanite. N Jahrb Mineral Monatsh 97–103

Černý P, Novák, Chapman R (1995) The Al(Nb, Ta)Ti_{-2} substitutions in titanite: the emergence of a new species ? Mineral Petrol 52:61–73

Chakhmouradian AR (2004) Crystal chemistry and paragenesis of compositionally-unique (Al-, Fe-, Nb-, and Zr-rich) titanite from Afrikanda, Russia. Am Mineral 89:1752–1762

Chakhmouradian AR, Reguir EP, Mitchell RH (2003) Titanite in carbonatitic rocks: genetic dualism and geochemical significance. Per Mineral 72(Special issue Eurocarb):107–113

Cheary RW, Cline PC (1995) An analysis of the effect of the different instrumental conditions on the shapes of X-ray powder line profiles. Adv X-ray Anal 38:75–82

Chiari C, Gazzoni G, Craig JR, Gibbs GV, Lousnathan SJ (1985) Two independent refinements of the structure of paracelsian, $BaAl_2Si_2O_8$. Am Mineral 70:969–974

Clark AM (1974) A tantalum-rich variety of sphene. Mineral Mag 39:605–607

Della Ventura G, Bellatreccia F, Williams CT (1999) Zr- and *LREE*-rich titanite from Tre Croci, Vico Volcanic complex (Latinum, Italy). Mineral Mag 63:123–130

Elleman-Olesen R, Malcherek T (2005) Temperature and composition dependence of structural phase transitions in $Ca(Ti_{1-x}Zr_x)OGeO_4$. Am Mineral 90:687–694

Ghose S, Yoshiaki I, Hatch DM (1991) Paraelectric–antiferroelectric phase transition in titanite, $CaTiSiO_5$. I. A high-temperature X-ray diffraction study of the order parameter and transition mechanism. Phys Chem Mineral 17:591–603

Ghose S, McMullan RK, Weber HP (1993) Neutron diffraction studies of the $P\bar{1} - I\bar{1}$ transition in anorthite, $CaAl_2Si_2O_8$ and the crystal structure of the body-centered phase at 514 K. Z Kristallogr 204:215–237

Griffen DT, Ribbe PH, Gibbs GV (1977) The structure of slawsonite, a strontium analog of paracelsian. Am Mineral 62:31–35

Hughes JM, Bloodaxe ES, Hanchar JM, Foord EE (1997) Incorporation of rare earth elements in titanite: stabilization of the $A2/a$ dimorph by creation of antiphase boundaries. Am Mineral 82:512–516

Kek S, Aroyo M, Bismayer U, Schmidt C, Eichhorn K, Krane HG (1997) The two-step phase transition of titanite, $CaTiSiO_5$: a synchrotron radiation study. Zeitschrift Krist 212:9–19

Kunz M, Brown ID (1994) Out-of-center distortions around octahedrally coordinated d^0-transition metals. J Solid State Chem 115:395–406

Kunz M, Xirouchakis D, Lindsley DH, Häusermann D (1996) High-pressure phase transition in titanite ($CaTiOSiO_4$). Am Mineral 81:1527–1530

Kunz M, Xirouchakis D, Yanbing Wang, Parise JB, Lindsley DH (1997) structural investigations along the join $CaTiOSiO_4$–$CaSnOSiO_4$. Schweiz Mineral Petr Mittel 77:1–11

Kunz M, Arlt T, Stolz J (2000) In situ powder diffraction study of titanite ($CaTiOSiO_4$) at high pressure and high temperature. Am Mineral 85:1465–1473

Liferovich RP, Mitchell RH (2005a) Composition and paragenesis of Na-, Nb- and Zr-bearing titanite from Khibina, Russia, and crystal-structure data for synthetic analogues. Can Mineral 43:795–812

Liferovich RP, Mitchell RH (2005b) Crystal chemistry of titanite-structured compounds: the $CaTi_{1-x}Zr_xOSiO_4$ ($x \le 0.5$) series. Phys Chem Mineral 32:40–51

Liferovich RP, Mitchell RH (2005c) Solid solution of rare earth elements in synthetic titanite: a reconnaissance study. Mineral Petrol 83:271–282

Malcherek T (2001) Spontaneous strain in synthetic titanite, $CaTiOSiO_4$. Mineral Mag 65:709–715

Paul BJ, Černý BJ, Chapman R, Hinthorne JR (1981) Niobian titanite from the Huron claim pegmatite, Southeastern Manitoba. Can Mineral 19:549–552

Robinson K, Gibbs GV, Ribbe PH (1971) Quadratic elongation: a quantitative measure of distortion in coordination polyhedra. Science 172:567–570

Rossi G, Oberti R, Smith DC (1986) Crystal structure of lisetite, $CaNa_2Al_4Si_4O_{16}$. Am Mineral 71:1378–1383

Russel JK, Groat LA, Halleran AAD (1994) *LREE*-rich niobian titanite from Mount Bisson, British Columbia: chemistry and exchange mechanisms. Can Mineral 32:575–587

Sahama TG (1946) On the chemistry of mineral titanite. CR Soc Geol Finlande 19 139:88–120

Salje E, Schmidt C, Bismayer U (1993) Structural phase transitions in titanite, $CaTiSiO_5$: a Raman spectroscopic study. Phys Chem Mineral 19:502–506

Shannon RD (1976) Revised effective ionic radii and systematic studies of interatomic distances in halides and chalcogenides. Acta Crystallogr A32:751–767

Speer JA, Gibbs GV (1976) The crystal structure of synthetic titanite, $CaTiOSiO_4$, and the domain textures of natural titanites. Am Mineral 61:238–247

Tait KT, Sokolova E, Hawthorne FC, Khomyakov AP (2003) The crystal chemistry of nepheline. Can Mineral 41:61–70

Taylor M, Brown GE (1976) High-temperature structural study of the $P2_1/a \leftrightarrow A2/a$ phase transition in synthetic titanite, $CaTiSiO_5$. Am Mineral 61:435–437

Troitzsch U, Ellis DJ (2002) Thermodynamic properties and stability of AlF-bearing titanite $CaTiOSiO_4$–$CaAlFSiO_4$. Contrib Mineral Petrol 142:543–563

Troitzsch U, Ellis DJ, Thompson J, FitzGerald JD (1999) Crystal structural changes in titanite along the join TiO–AlF. Eur J Mineral 6:955–965

Van Heurk C, van Tendeloo G, Ghose S, Amelinckx S (1991) Paraelectric–antiferroelectric phase transition in titanite, $CaTiSiO_5$. II. Electron diffraction and electron microscopic studies of the transition dynamics. Phys Chem Mineral 17:604–610

Wainwright JE, Starkey J (1971) A refinement of the structure of anorthite. Z Kristallogr 133:75–84

Woolley AR, Platt RG, Eby N (1992) Niobian titanite and eudialyte from the Ilomba nepheline syenite complex, North Malawi. Mineral Mag 56:428–430

Young RA (ed) (1995) The Rietveld method. Oxford University Press, New York, 298 pp